

Supplementary data for article:

Marković, V.; Markovic, S.; Janicijevic, A.; Rodić, M.; Leovac, V. M.; Todorović, N.; Trifunović, S. S.; Joksović, M. D. Mechanistic Investigation and DFT Calculation of the New Reaction between S-Methylisothiosemicarbazide and Methyl Acetoacetate. *Structural Chemistry* **2013**, 24 (6), 2127–2136. <https://doi.org/10.1007/s11224-013-0223-3>

STRUCTURAL CHEMISTRY

SUPPLEMENTARY DATA

associated with the paper

**Mechanistic investigation and DFT calculation of the
new reaction between *S*-methylothiosemicarbazide
and methyl acetoacetate**

Contents:

1. 1D NMR spectra of 16	S3
2. 1D and 2D NMR spectra of 3-methyl-5-oxo-3-pyrazolin-1-carboxamide (MOPC, 1)	S5
3. Experimental and calculated geometrical parameters of MOPC (1)	S13
4. Mechanism B : Elementary steps in the conversion of methyl acetoacetate <i>S</i> -methylisothiosemicarbazone (2b) into 1	S17
5. Mechanism A : Elementary steps in the hypothetical conversion of methyl acetoacetate <i>S</i> -methylisothiosemicarbazone (2b) into 3-aminopyrazole derivative 7	S22
6. Mechanism B : Elementary steps in the hypothetical conversion of acetylacetone mono- <i>S</i> -methylisothiosemicarbazone (2a) into 1	S25

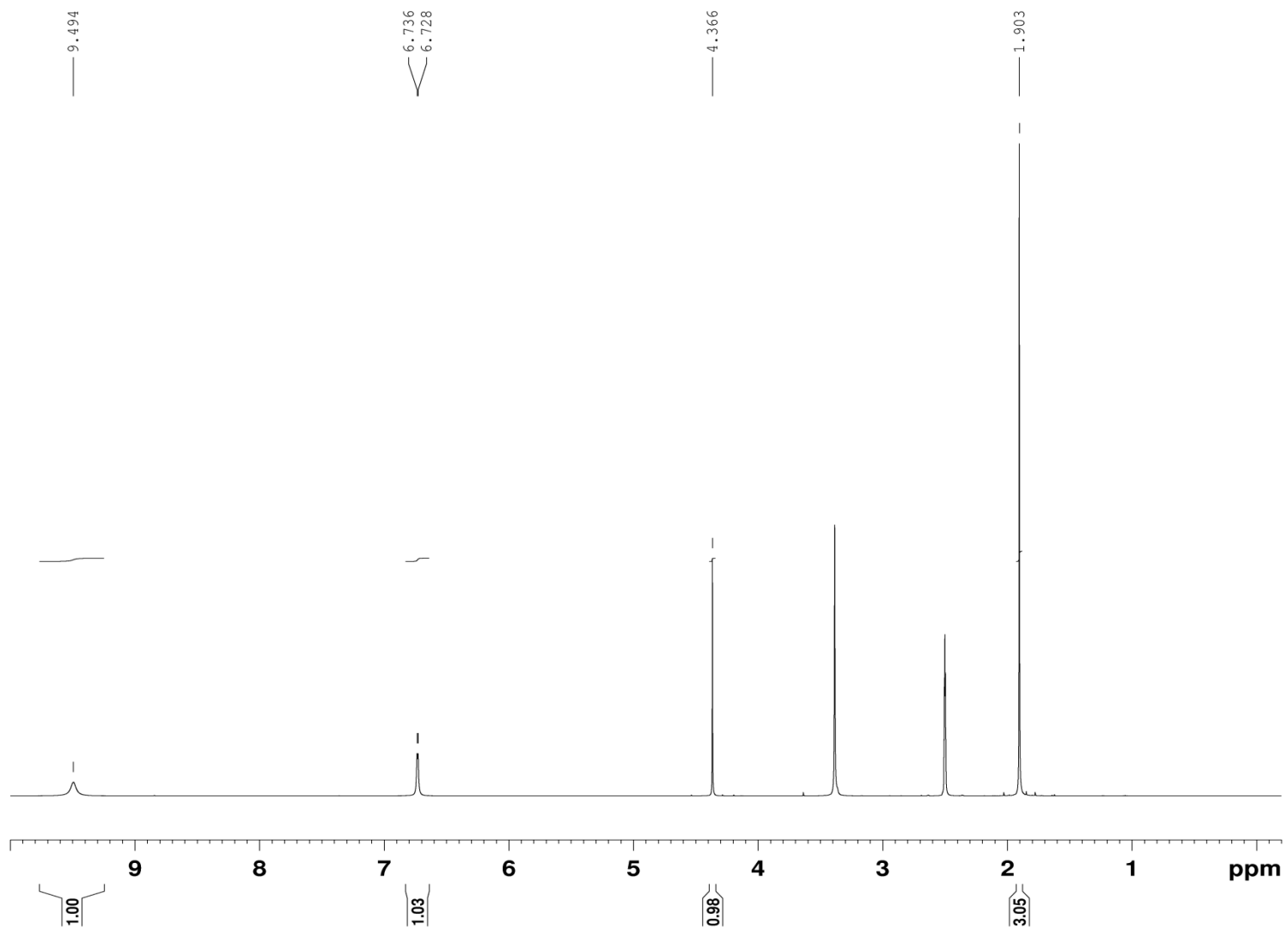


Fig. S1. ^1H NMR spectrum of **16**.

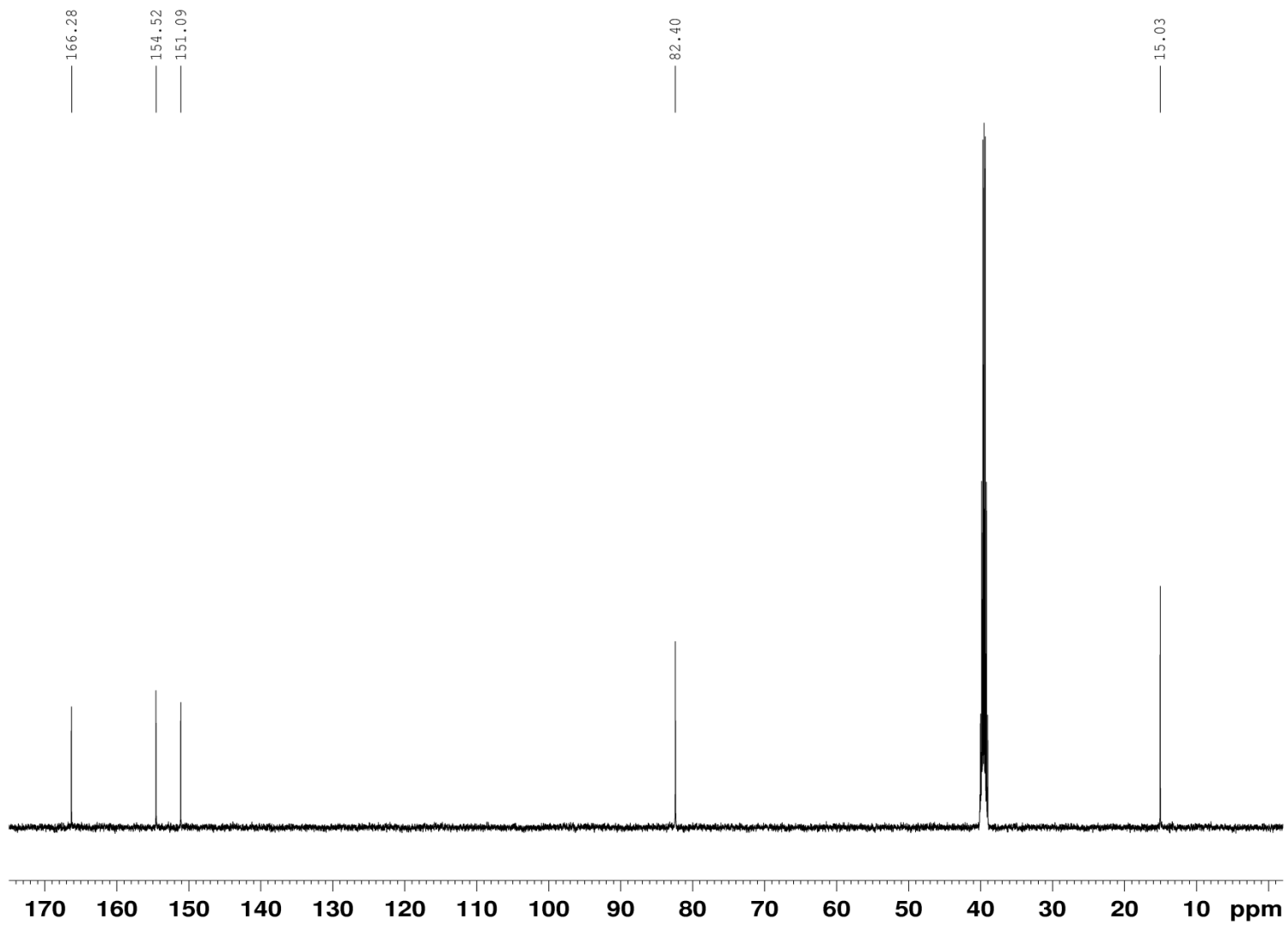


Fig. S2. ^{13}C NMR spectrum of **16**.

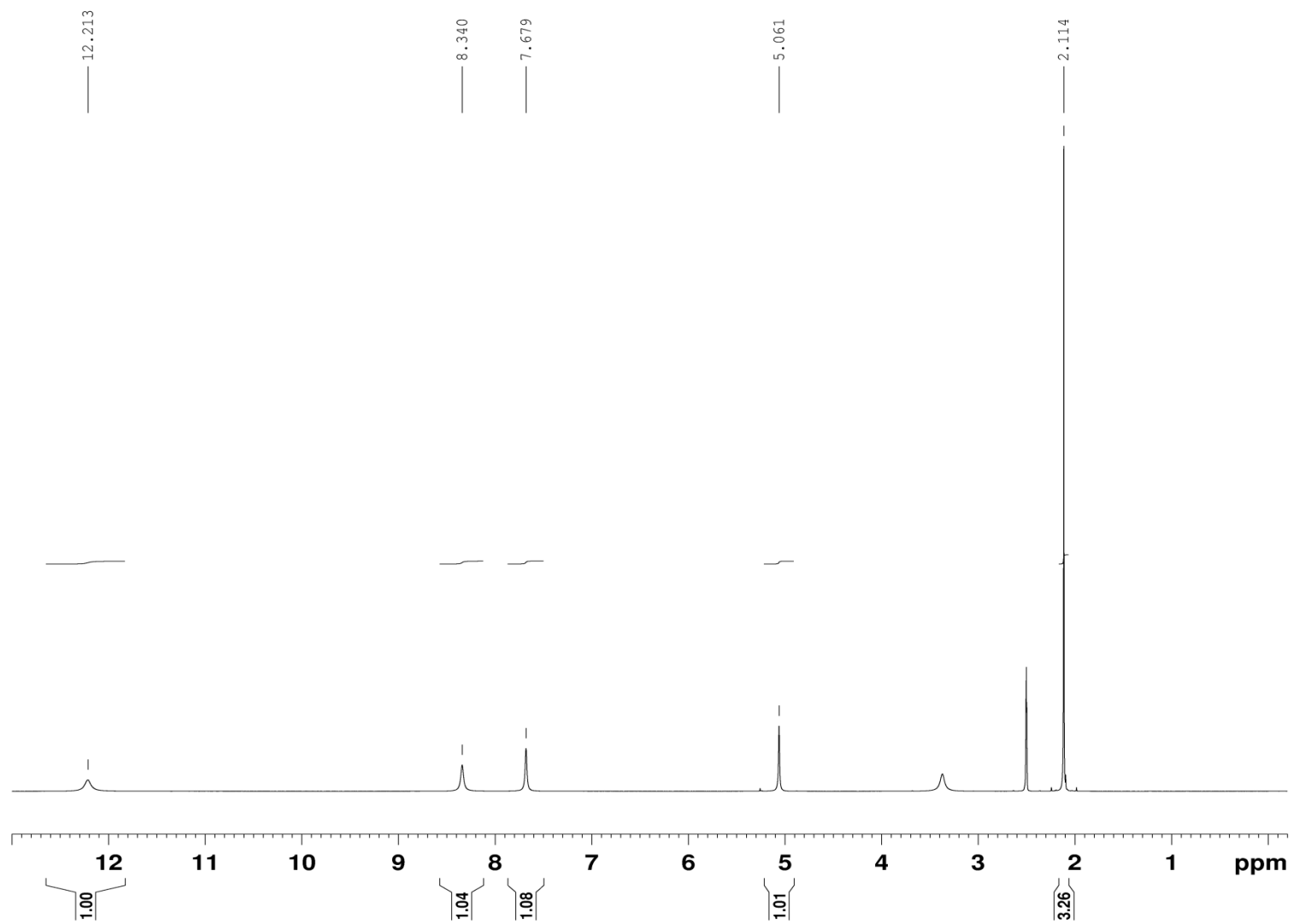


Fig. S3. ^1H NMR spectrum of **1**.

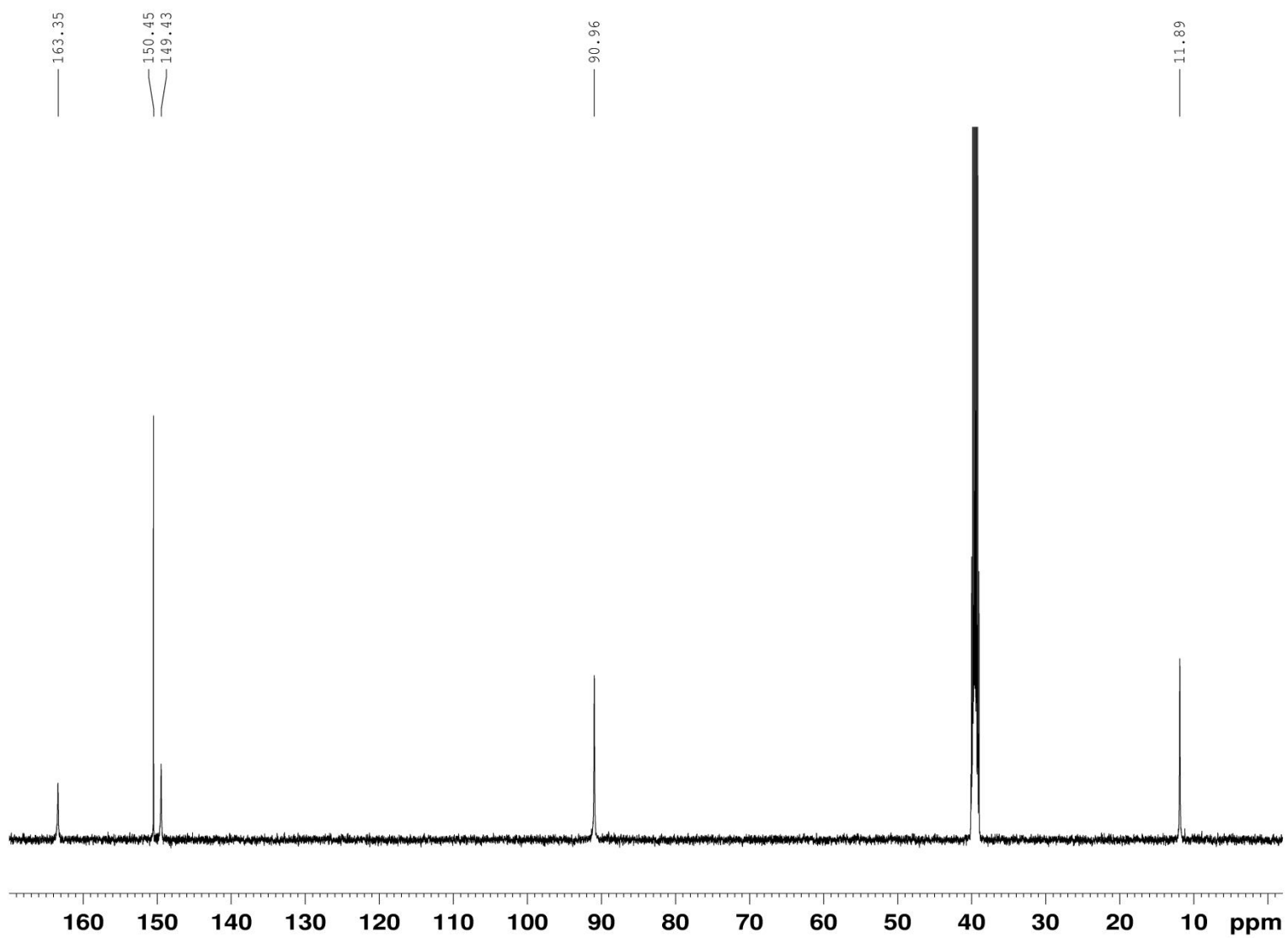


Fig. S4. ^{13}C NMR spectrum of **1**.

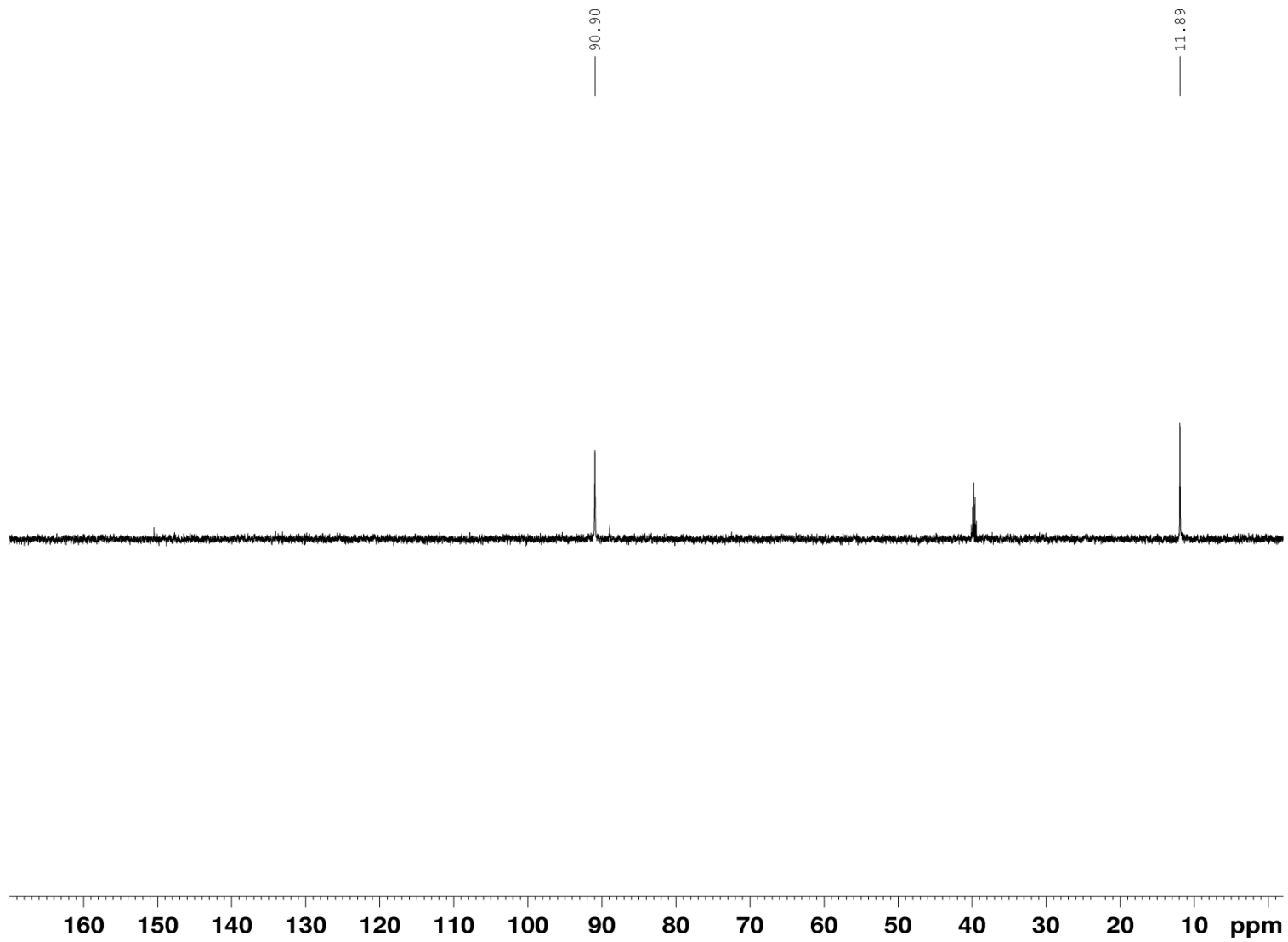


Fig. S5. DEPT spectrum of 1.

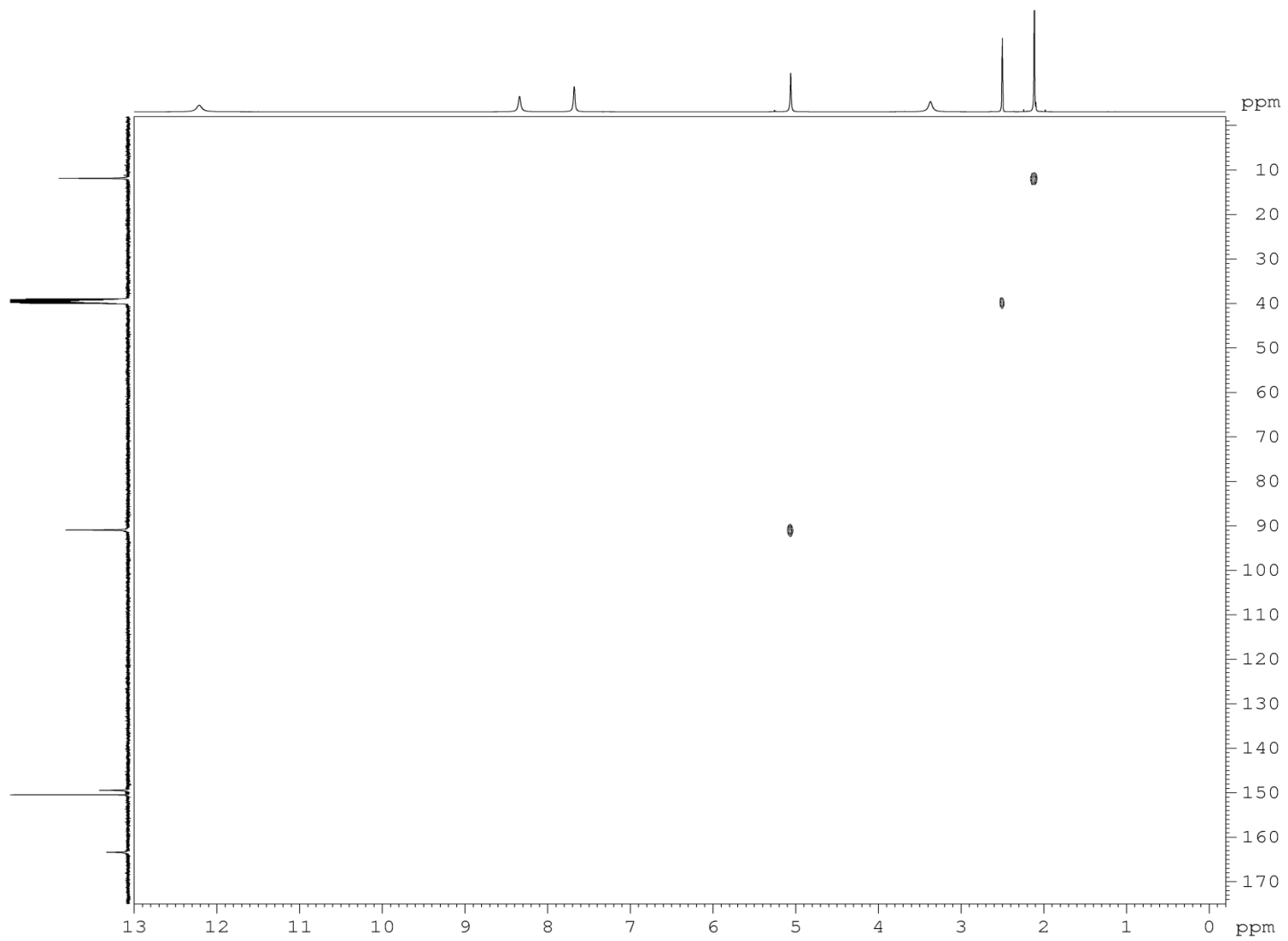


Fig. S6. HSQC spectrum of **1**.

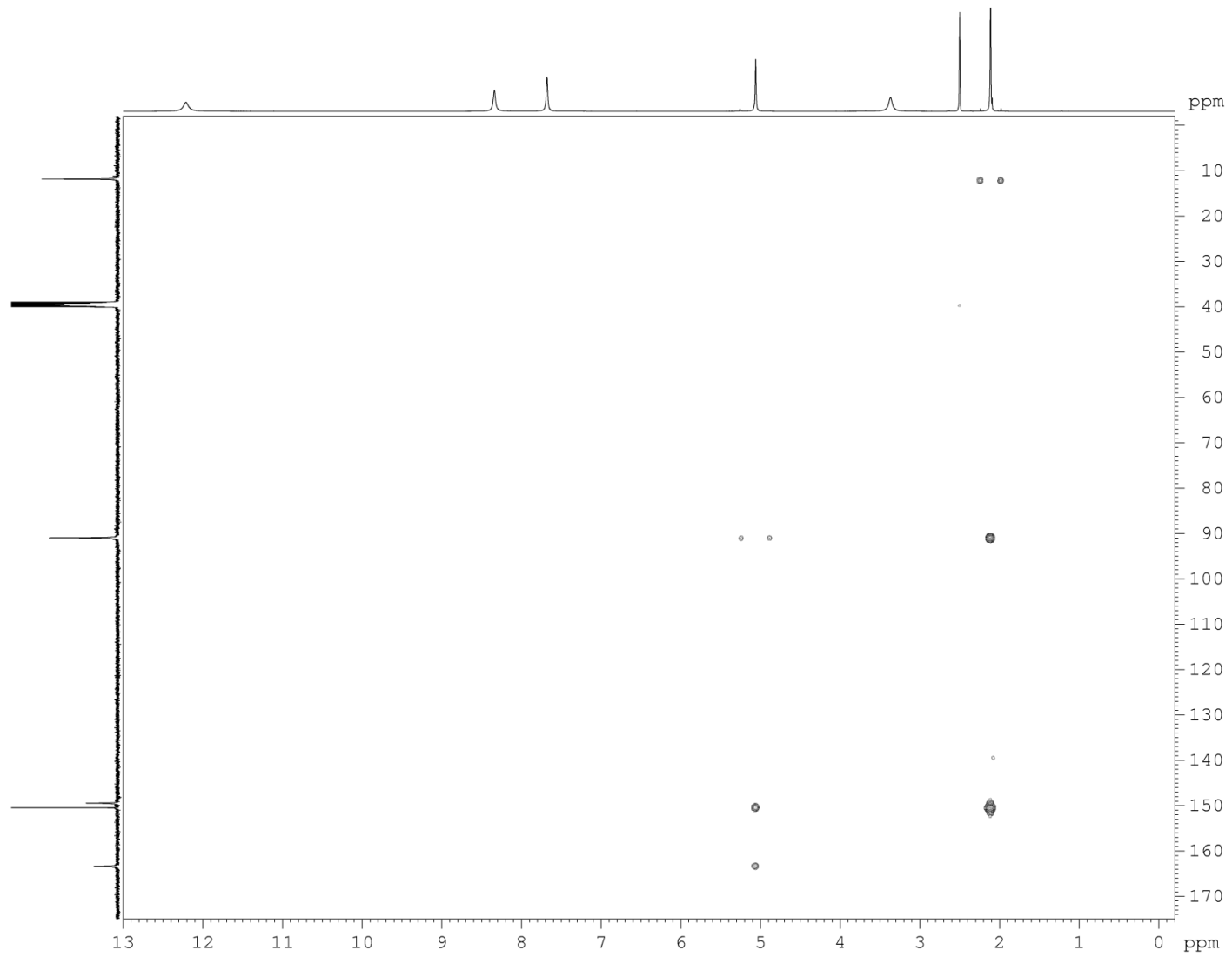


Fig. S7. HMBC spectrum of **1**.

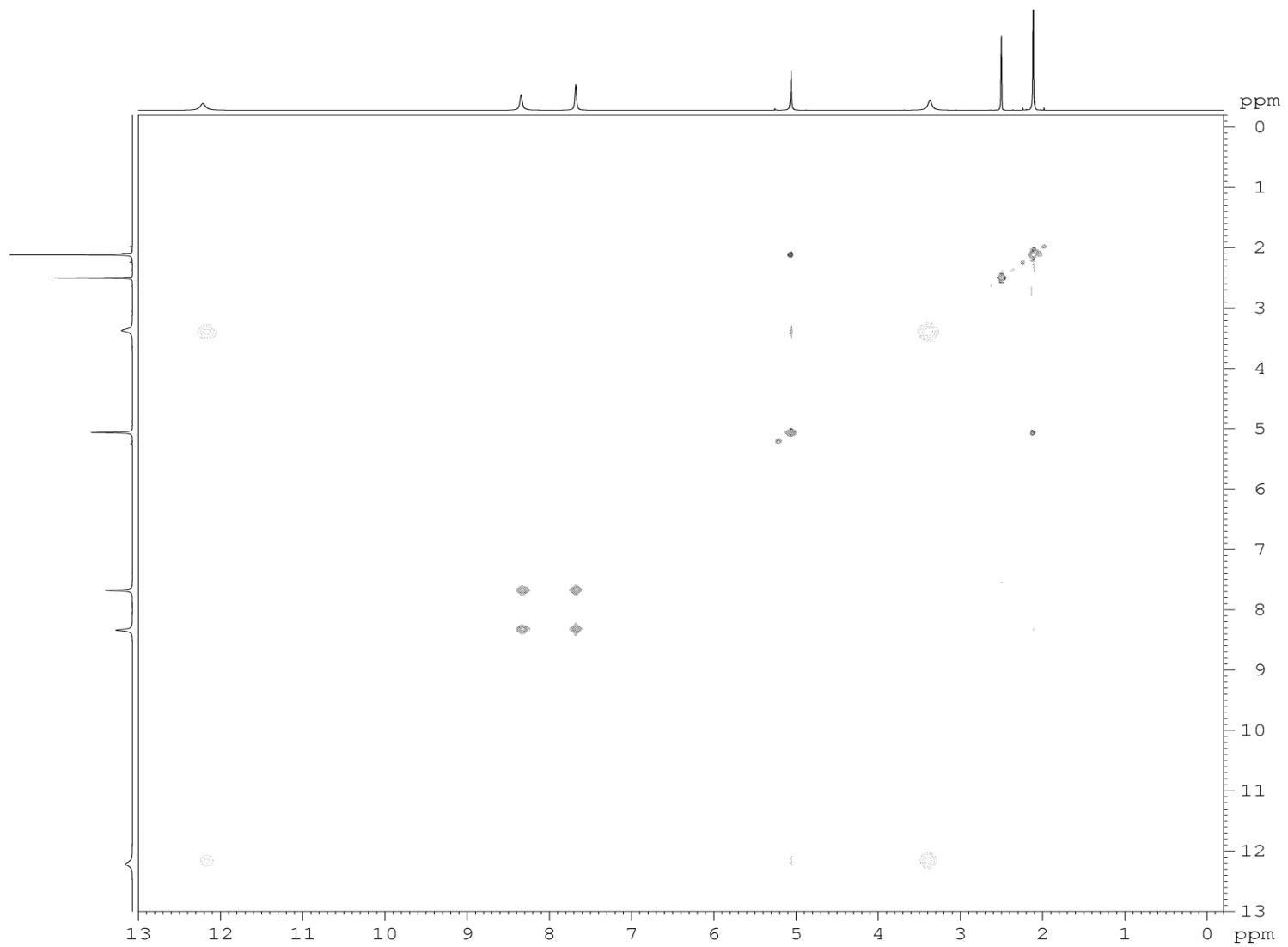


Fig. S8. NOESY spectrum of **1**.

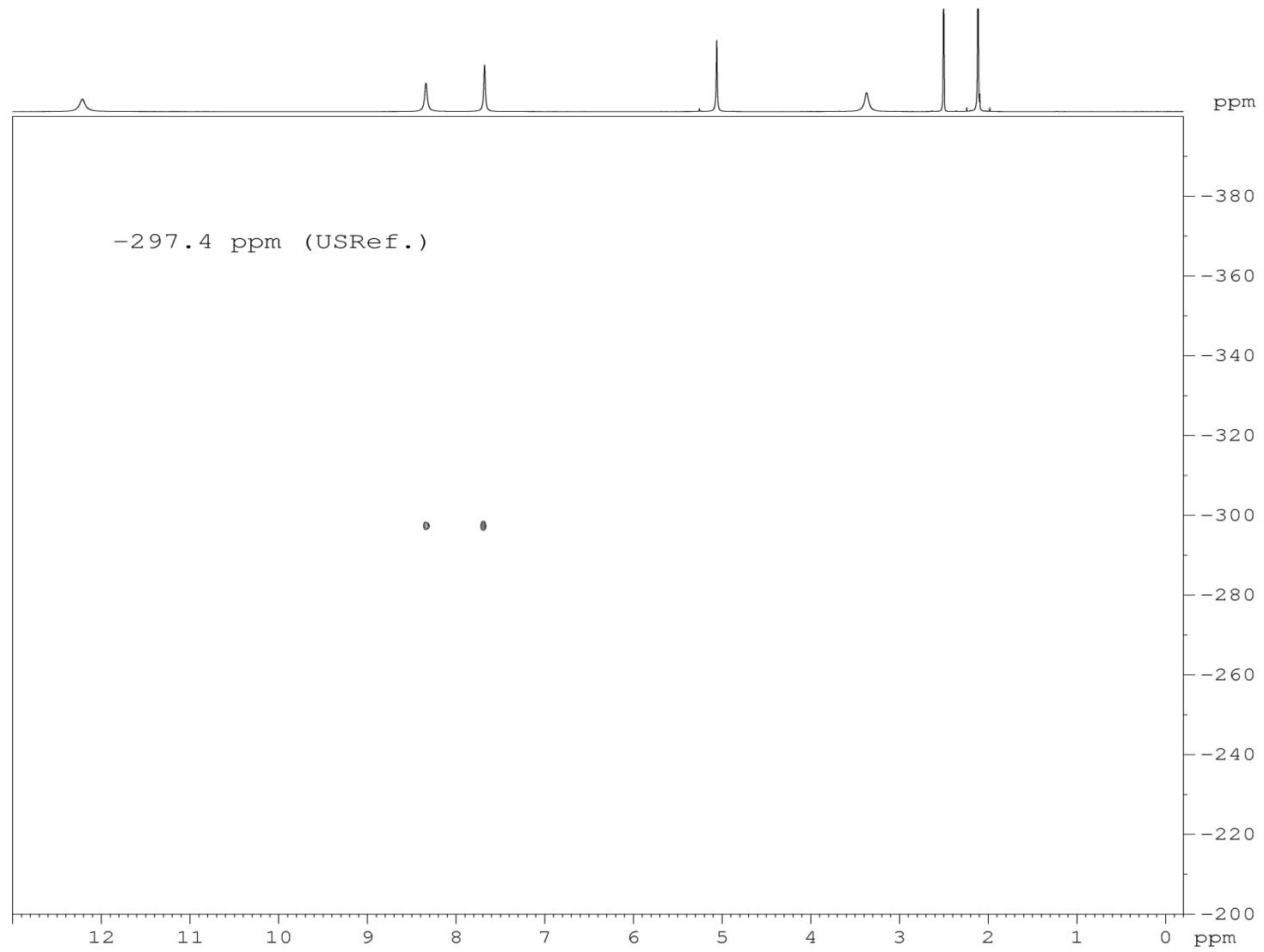


Fig. S9. ^1H - ^{15}N HSQC spectrum of **1**.

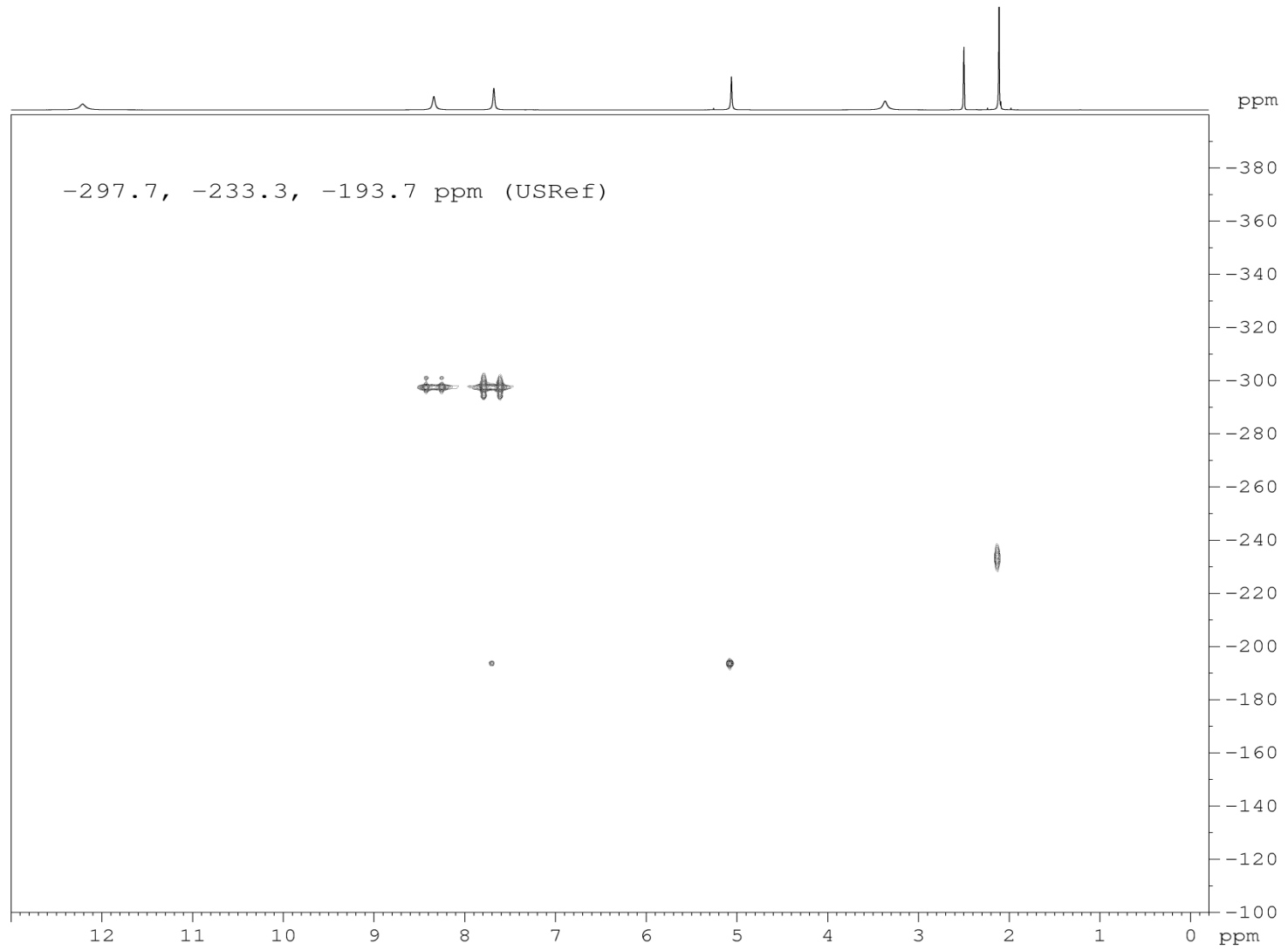


Fig. S10. ^1H - ^{15}N HMBC spectrum of **1**.

Experimental and calculated geometrical parameters of MOPC (1)

Table S1. Experimental and calculated bond lengths (Å) in **1**.

Bond length	Experimental	Calculated
O2—C7	1.220 (2)	1.225
C6—C3	1.487 (2)	1.490
C6—H4D	0.96	1.089
C6—H4E	0.96	1.093
C6—H4F	0.96	1.093
C7—N3	1.320 (2)	1.344
C7—N1	1.408 (2)	1.411
N1—N2	1.368 (2)	1.385
N1—C5	1.400 (2)	1.418
N2—C3	1.334 (2)	1.364
N2—H2	0.88 (2)	1.013
C3—C4	1.367 (2)	1.372
O1—C5	1.247 (2)	1.239
C4—C5	1.407 (2)	1.435
C4—H4	0.93	1.077
N3—H3A	0.86 (3)	1.016
N3—H3B	0.85 (3)	1.007

Table S2. Experimental and calculated bond angles (°) in **1**.

Bond angle	Experimental	Calculated
C3—C6—H4D	109.5	110.1
C3—C6—H4E	109.5	110.7
H4D—C6—H4E	109.5	108.8
C3—C6—H4F	109.5	110.8
H4D—C6—H4F	109.5	108.6
H4E—C6—H4F	109.5	107.8
O2—C7—N3	127.0 (2)	126.6
O2—C7—N1	118.5 (2)	119.7
N3—C7—N1	114.4 (2)	113.7
N2—N1—C5	109.2 (1)	109.3
N2—N1—C7	120.1 (1)	118.9
C5—N1—C7	130.6 (2)	131.6
C3—N2—N1	108.4 (1)	108.0
C3—N2—H2	127.9 (1)	125.7
N1—N2—H2	123.0 (1)	116.4
N2—C3—C4	109.4 (2)	109.4
N2—C3—C6	120.2 (2)	120.4
C4—C3—C6	130.3 (2)	130.1
C3—C4—C5	108.4 (2)	108.6
C3—C4—H4	125.8	126.7
C5—C4—H4	125.8	124.6
C7—N3—H3A	120.7 (2)	119.7
C7—N3—H3B	118.6 (2)	118.5
H3A—N3—H3B	121 (2)	121.7
O1—C5—N1	121.8 (2)	123.1
O1—C5—C4	133.7 (2)	132.5
N1—C5—C4	104.5 (2)	104.3

Table S3. Experimental and calculated dihedral angles (°) in **1**.

Torsion angle	Experimental	Calculated
O2—C7—N1—N2	1.1 (2)	5.4
N3—C7—N1—N2	-178.3 (2)	-175.2
O2—C7—N1—C5	176.0 (2)	179.5
N3—C7—N1—C5	-3.4 (3)	-1.2
C5—N1—N2—C3	1.7 (2)	5.9
C7—N1—N2—C3	177.6 (2)	178.7
N1—N2—C3—C4	-1.2 (2)	-5.8
N1—N2—C3—C6	179.2 (2)	175.2
N2—C3—C4—C5	0.3 (2)	3.5
C6—C3—C4—C5	179.7 (2)	177.6
N2—N1—C5—O1	177.8 (2)	175.6
C7—N1—C5—O1	2.5 (3)	1.1
N2—N1—C5—C4	-1.5 (2)	-3.6
C7—N1—C5—C4	-176.8 (2)	-178.2
C3—C4—C5—O1	-178.5 (2)	-179.0
C3—C4—C5—N1	0.7 (2)	0.2

Table S4. Hydrogen-bond geometry (Å, °)

<i>D</i> —H··· <i>A</i>	<i>D</i> —H	H··· <i>A</i>	<i>D</i> ··· <i>A</i>	<i>D</i> —H··· <i>A</i>
N3—H3A···O1	0.86 (3)	2.03 (2)	2.701 (2)	135 (2)
N3—H3B···O2 ⁱ	0.85 (3)	2.09 (3)	2.930 (2)	168 (2)
N2—H2···O1 ⁱⁱ	0.88 (2)	1.83 (2)	2.711 (2)	172 (2)

Symmetry codes: (i) $-x+1, -y+1, -z$; (ii) $x-1, y, z$.

Table S5. Crystal data and refinement parameters

Molecular formula	C ₅ H ₇ N ₃ O ₂
CCDC No.	902014
<i>M</i> (g mol ⁻¹)	141.14
Color / habit	translucent pale pink / prism
Crystal size (mm)	0.29 × 0.24 × 0.08
Temperature (K)	298(2)
Crystal system	triclinic
Space group	<i>P</i> -1
<i>a</i> (Å)	6.0099(8)
<i>b</i> (Å)	7.3248(9)
<i>c</i> (Å)	7.602(1)
α (°)	90.11(1)
β (°)	100.81(1)
γ (°)	107.28(1)
<i>V</i> (Å ³)	313.30(7)
<i>Z</i>	2
<i>D</i> _{calc} (g cm ⁻³)	1.496
<i>F</i> (0 0 0)	148
θ range (°)	5.9–66.9
Data collection limits	$-7 \leq h \leq 7, -7 \leq k \leq 8, -9 \leq l \leq 9$
μ (mm ⁻¹)	1.01
<i>T</i> _{min} / <i>T</i> _{max}	0.891 / 1
Reflections collected	1676
Independent reflections	1120
<i>R</i> _{int}	0.021
Data [<i>F</i> _o > 4σ <i>F</i> _o]	934
Restraints / parameters	0 / 104
Goodness-of-fit on <i>F</i> ²	1.07
<i>R</i> / <i>wR</i> [<i>F</i> _o > 4σ <i>F</i> _o]	0.039 / 0.102
<i>R</i> / <i>wR</i> [all data]	0.047 / 0.11
$\Delta\rho_{\min}$ / $\Delta\rho_{\max}$ (e Å ⁻³)	-0.16 / 0.18

Mechanism B: Elementary steps in the conversion of methyl acetoacetate *S*-methylisothiosemicarbazone (2b) into 1

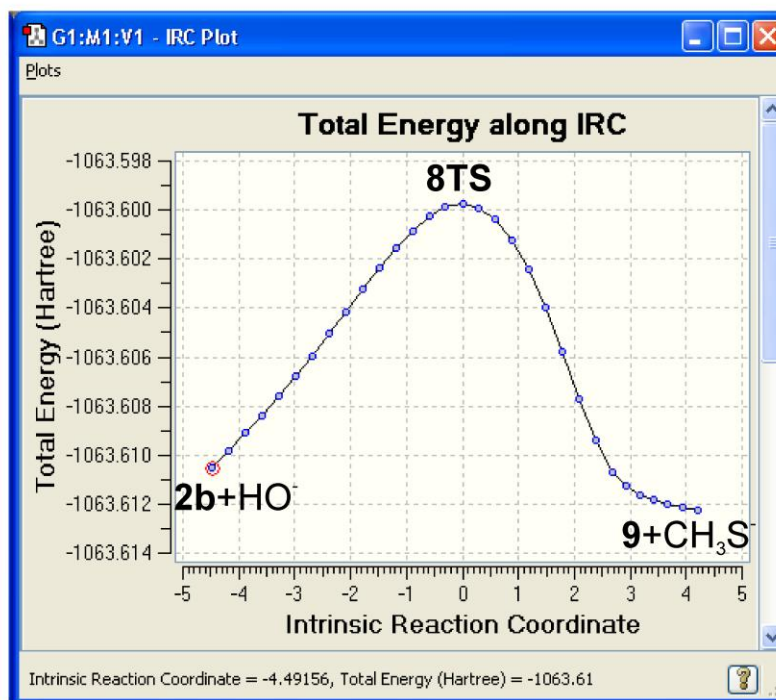
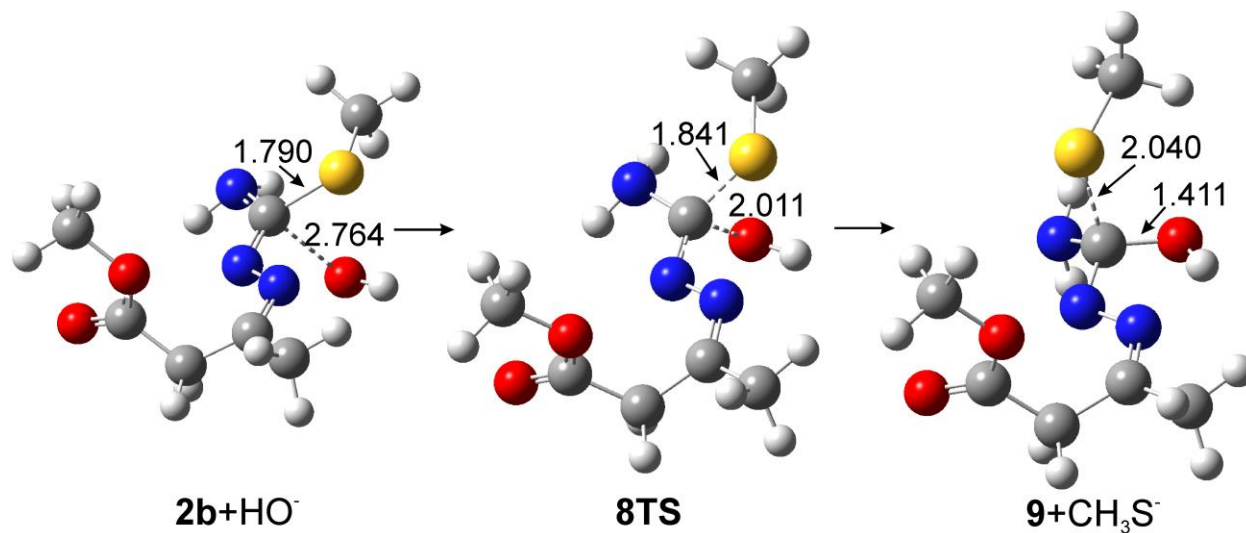


Fig. S11. Optimized geometries of the participants in step 1 with crucial intramolecular distances (Å), and results of the IRC calculation for related transition state.

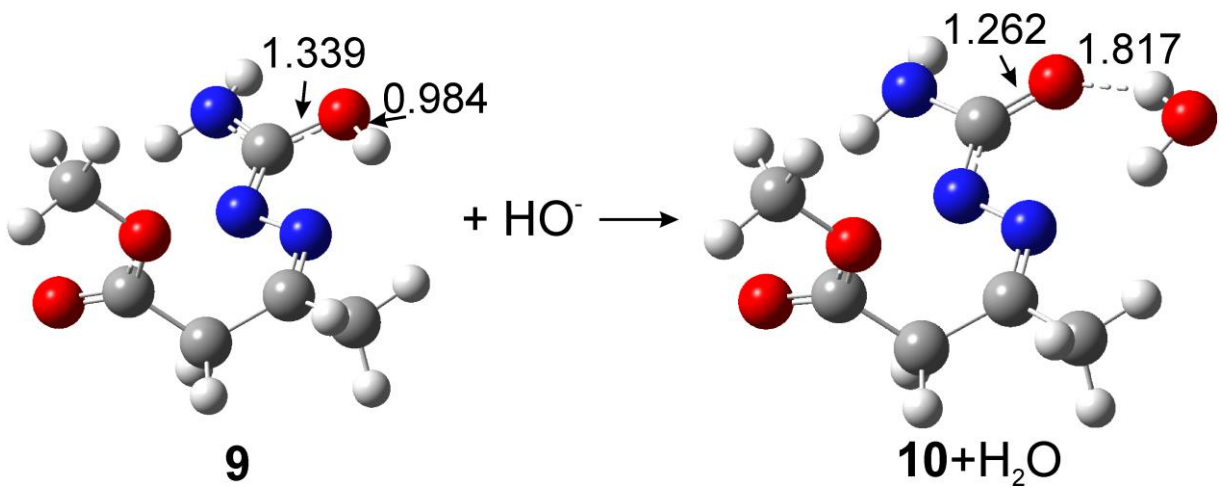


Fig. S12. Optimized geometries of the participants in step 2 with crucial intramolecular distances (Å).

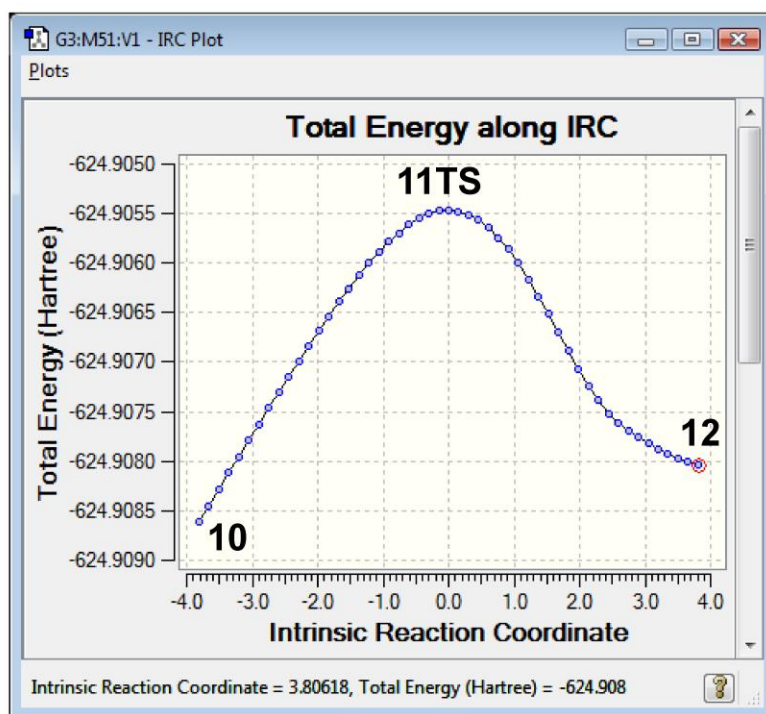
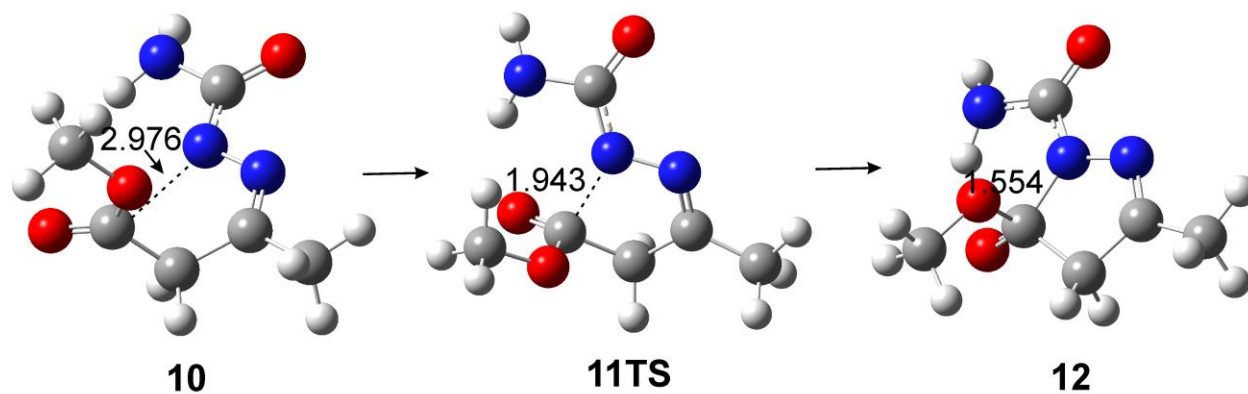


Fig. S13. Optimized geometries of the participants in step 3 with crucial intramolecular distances (Å), and results of the IRC calculation for related transition state.

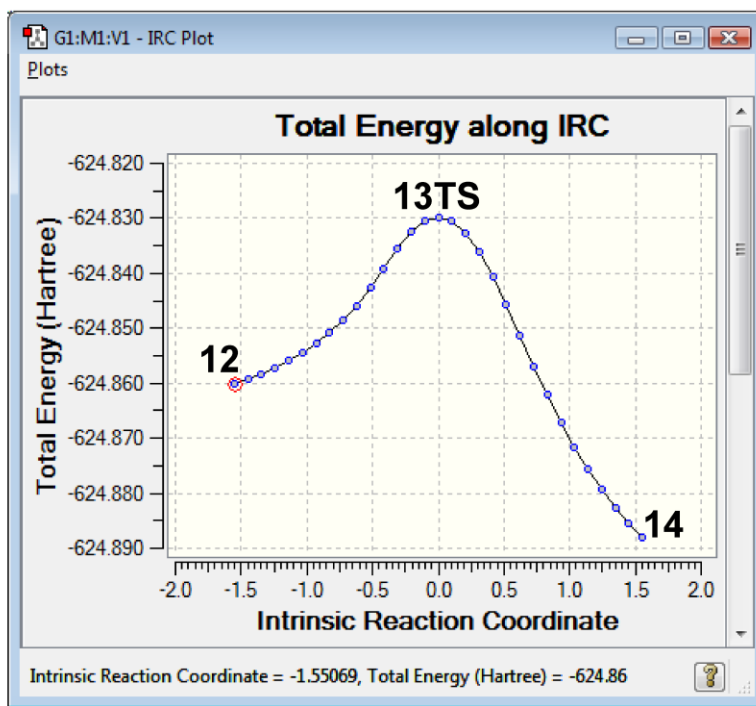
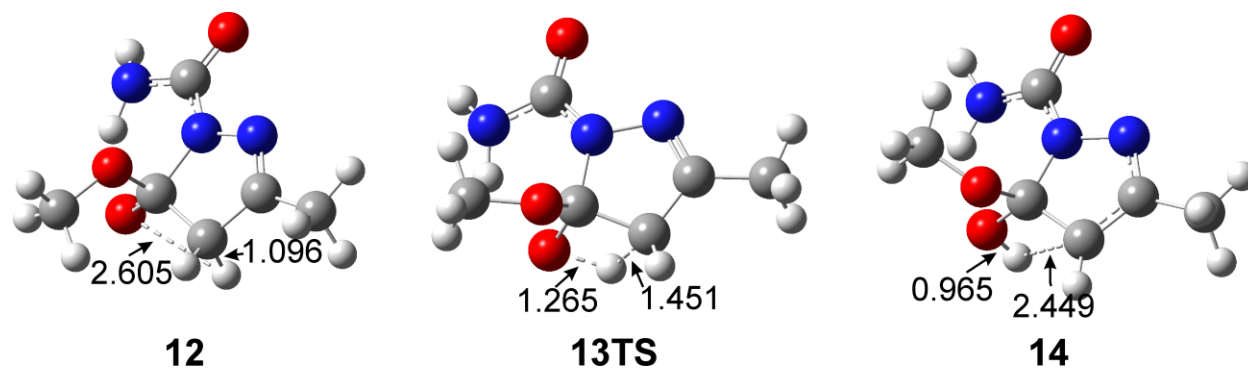


Fig. S14. Optimized geometries of the participants in step 4 with crucial intramolecular distances (Å), and results of the IRC calculation for related transition state.

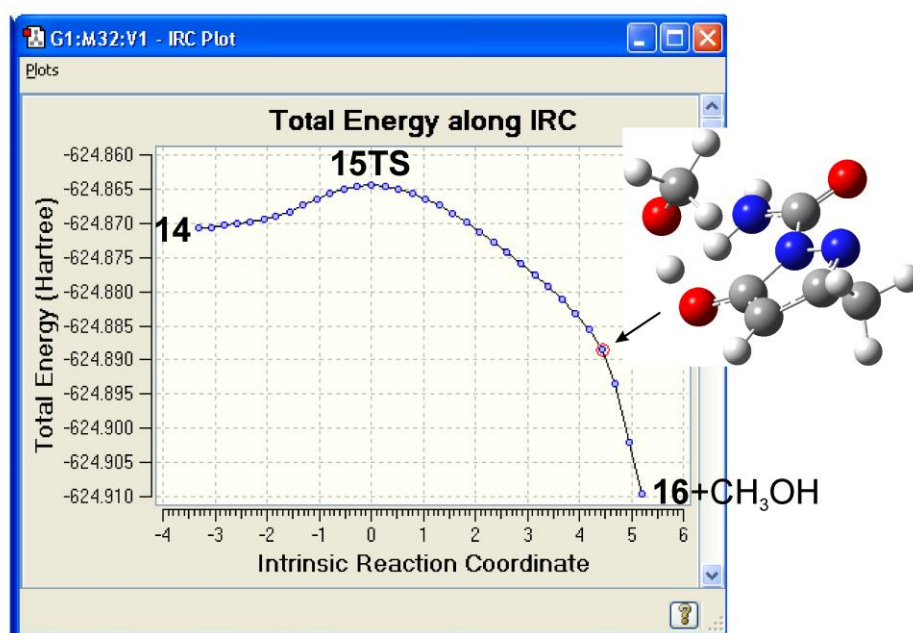
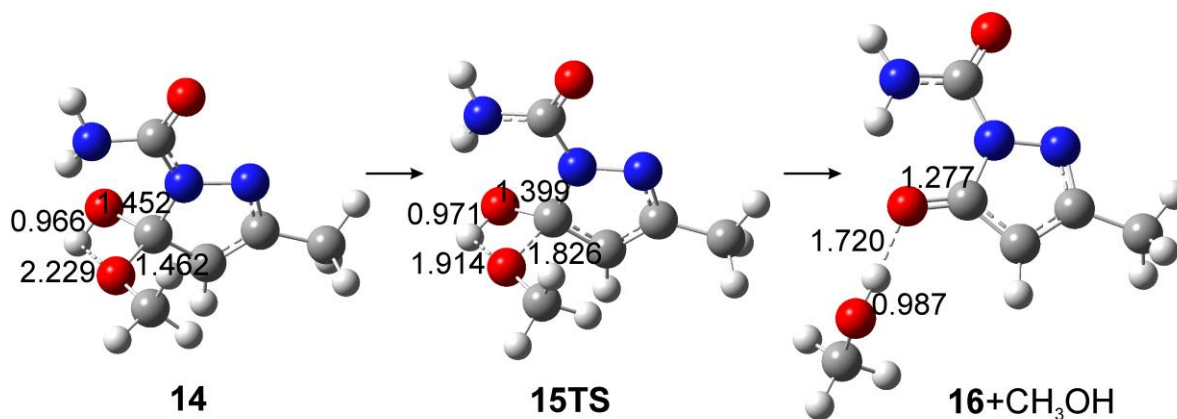


Fig. S15. Optimized geometries of the participants in step 5 with crucial intramolecular distances (Å), and results of the IRC calculation for related transition state.

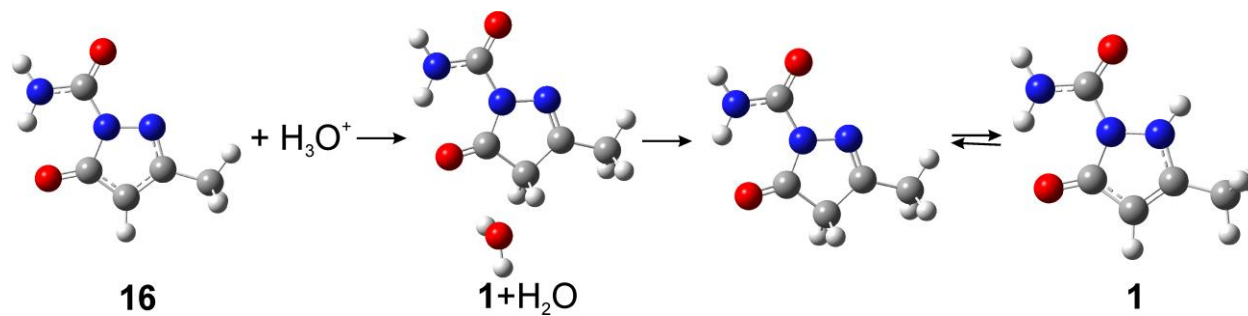


Fig. S16. Optimized geometries of the participants in step 6.

Mechanism A: Elementary steps in the hypothetical conversion of methyl acetoacetate *S*-methylisothiosemicarbazone (2b) into 3-aminopyrazole derivative 7

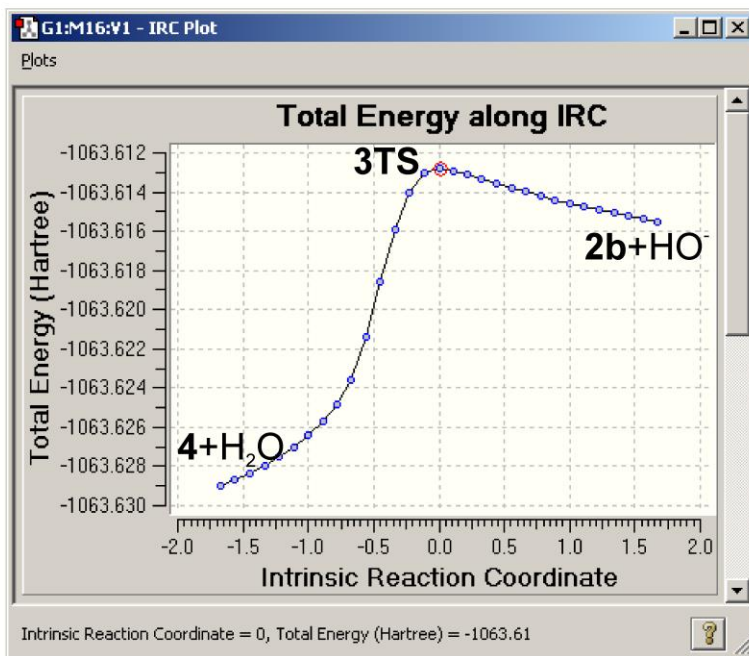
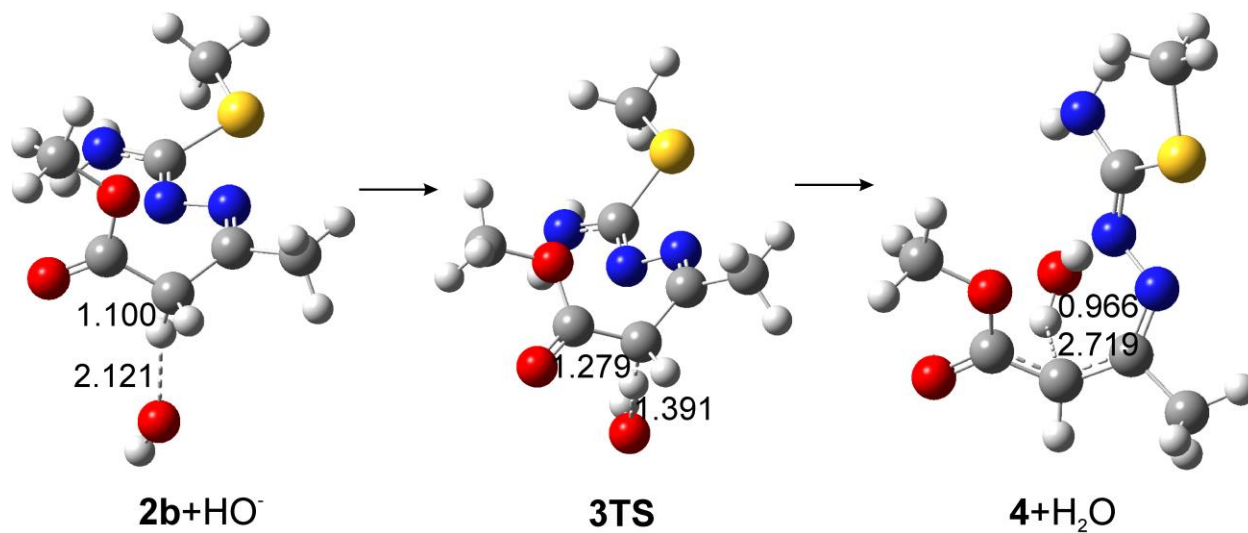


Fig. S17. Optimized geometries of the participants in step 1 with crucial intramolecular distances (Å), and results of the IRC calculation for related transition state.

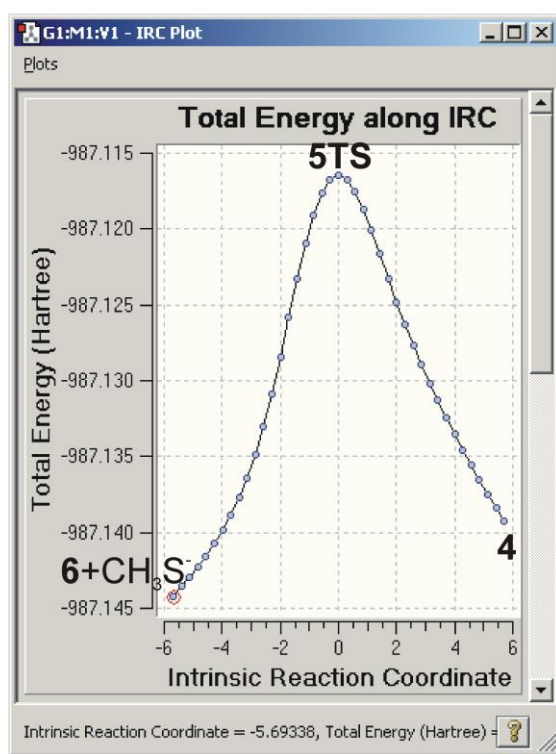
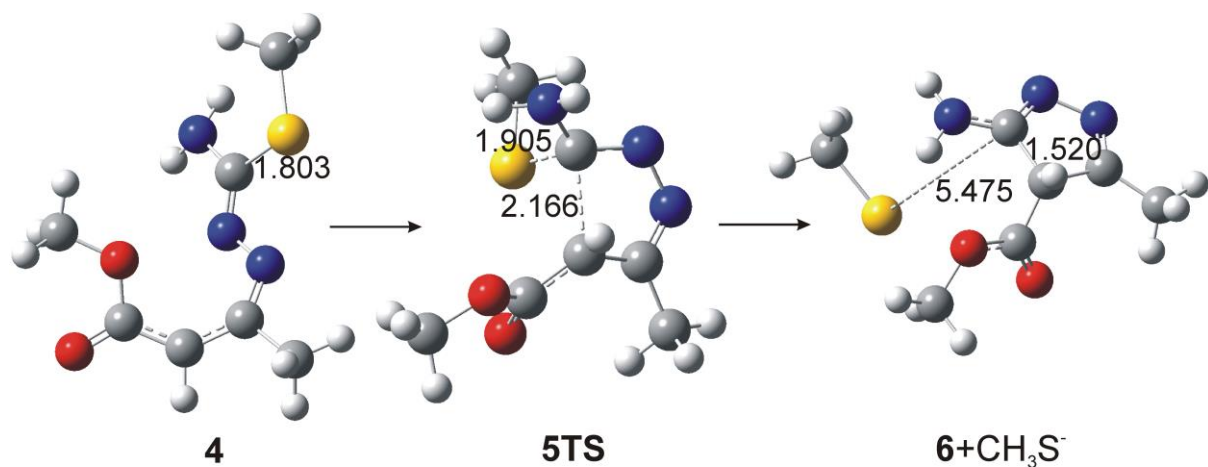


Fig. S18. Optimized geometries of the participants in step 2 with crucial intramolecular distances (Å), and results of the IRC calculation for related transition state.

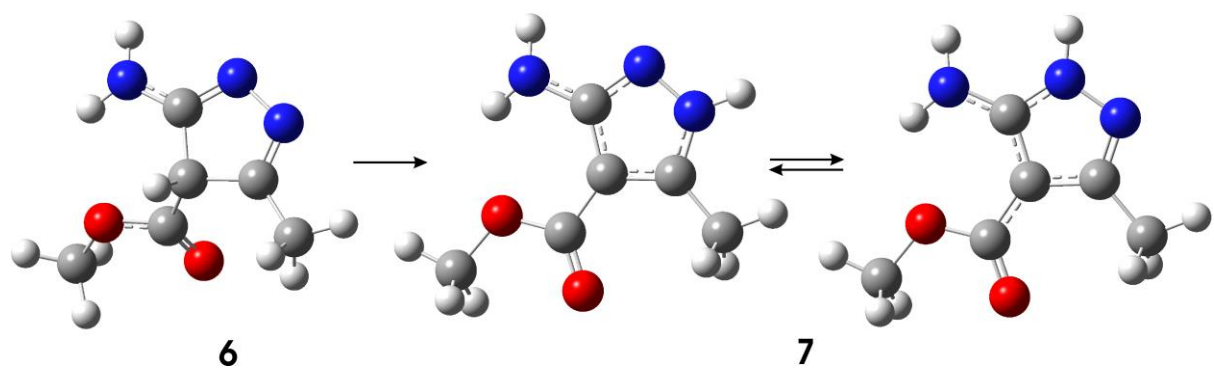


Fig. S19. Optimized geometries of the participants in step 3.

Mechanism B: Elementary steps in the hypothetical conversion of acetylacetonate mono-*S*-methylisothiosemicarbazone (2a) into 1

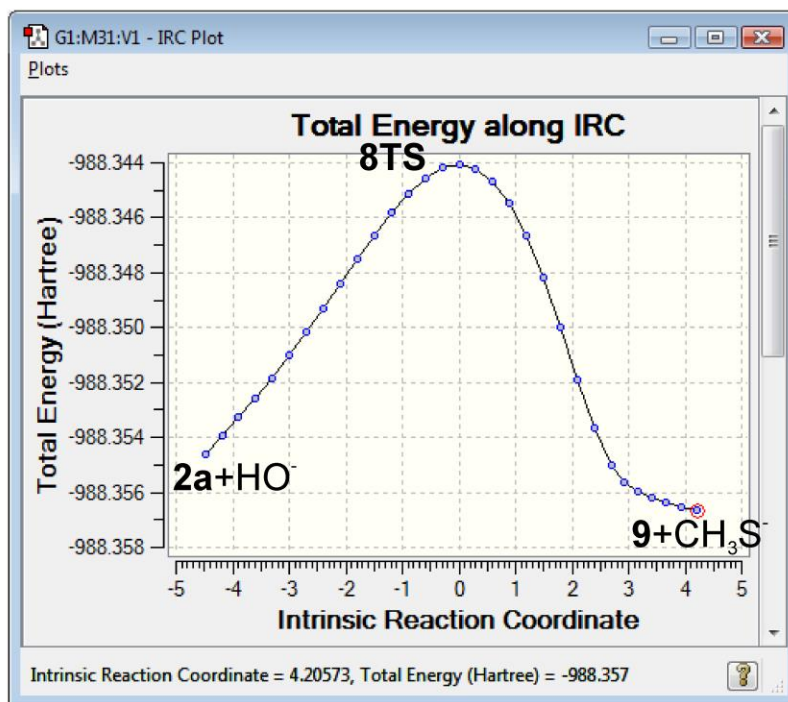
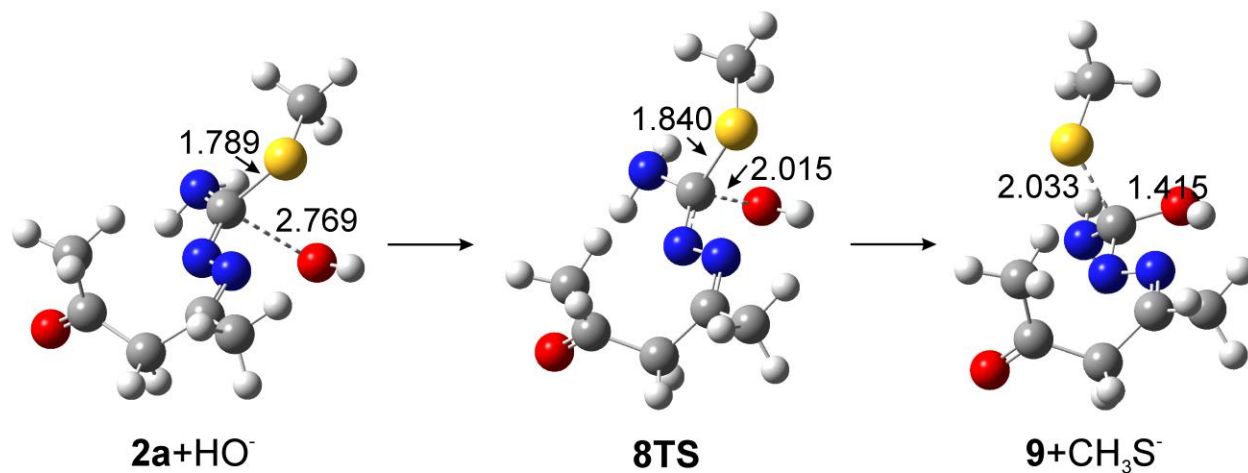


Fig. S20. Optimized geometries of the participants in step 1 with crucial intramolecular distances (Å), and results of the IRC calculation for related transition state.

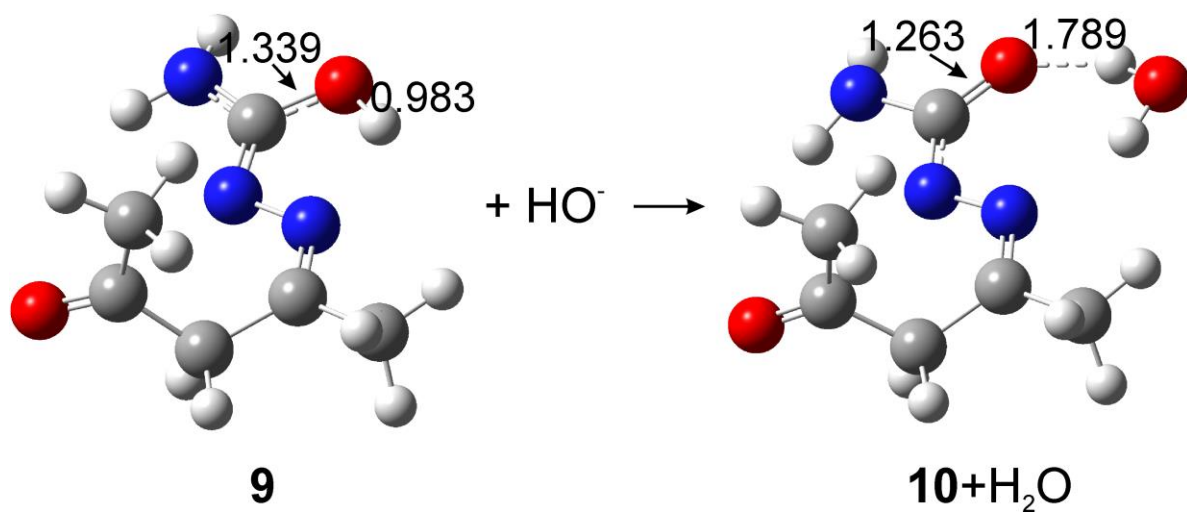


Fig. S21. Optimized geometries of the participants in step 2 with crucial intramolecular distances.

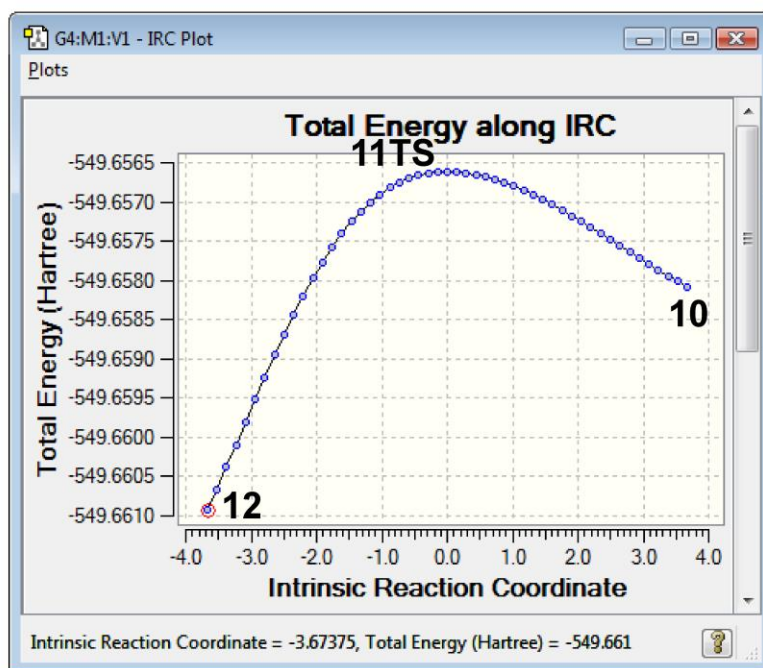
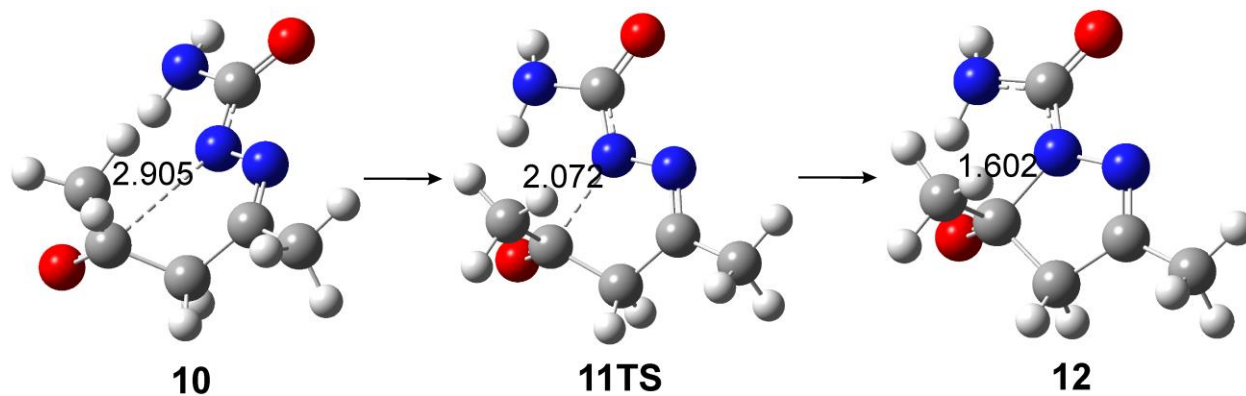


Fig. S22. Optimized geometries of the participants in step 3 with crucial intramolecular distances (Å), and results of the IRC calculation for related transition state.

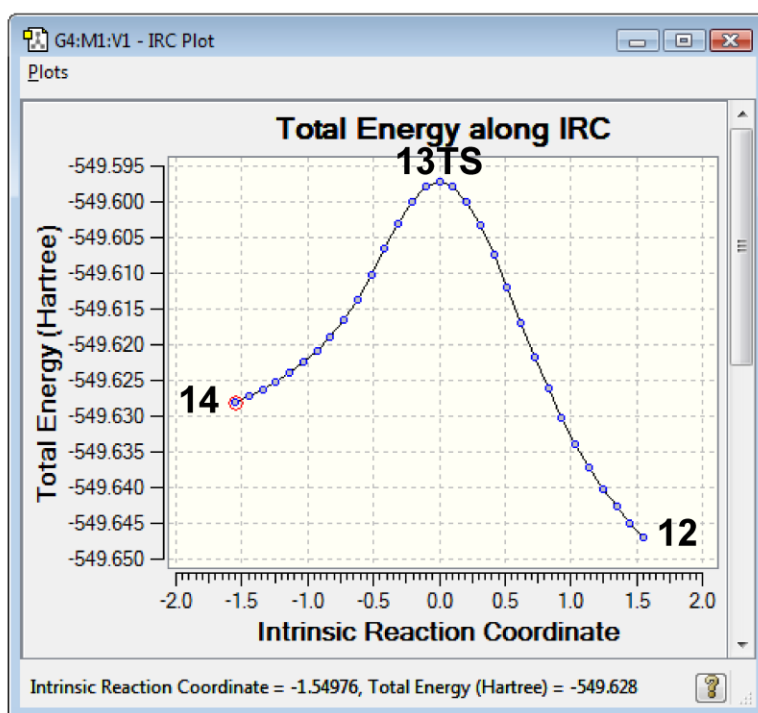
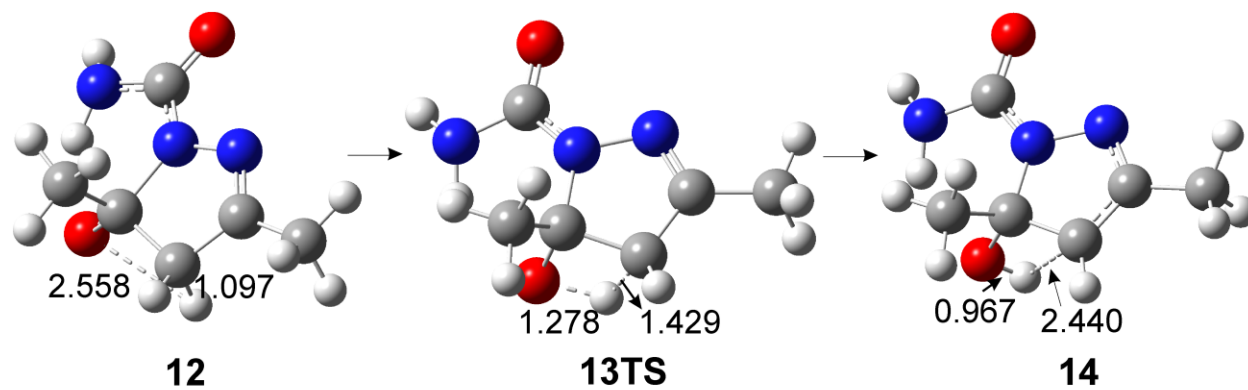


Fig. S23. Optimized geometries of the participants in step 4 with crucial intramolecular distances (Å), and results of the IRC calculation for related transition state.

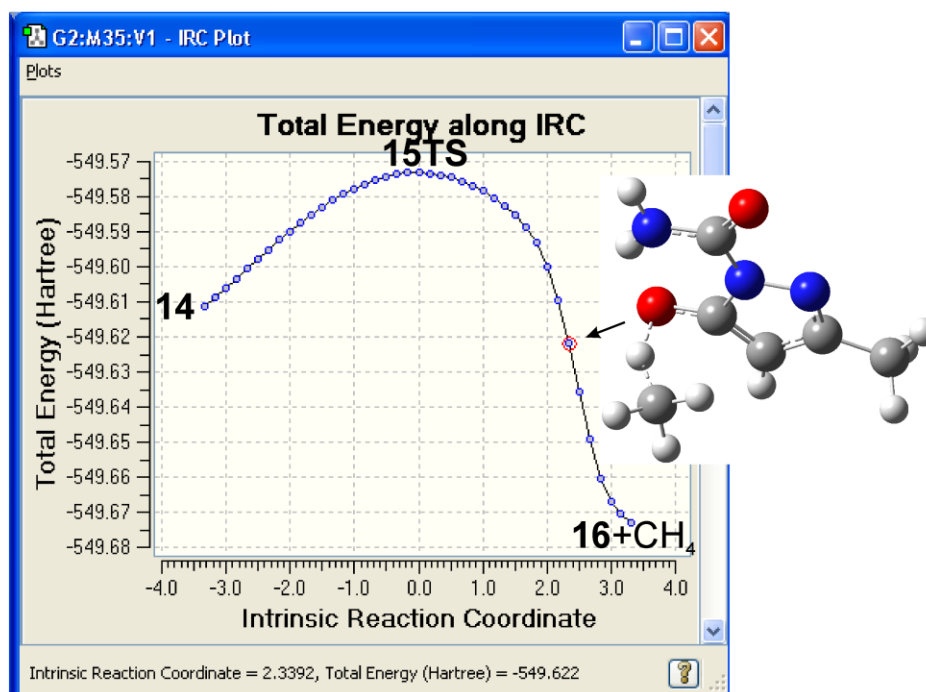
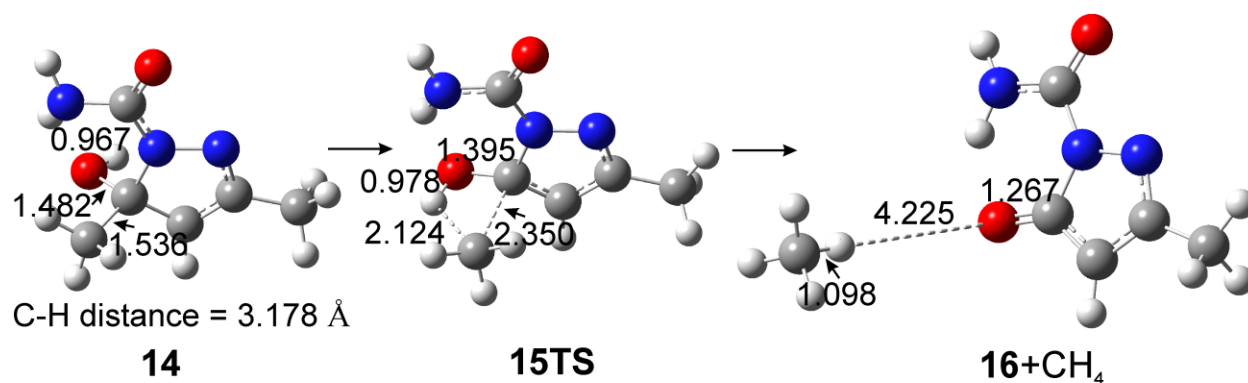


Fig. S24. Optimized geometries of the participants in step 5 with crucial intramolecular distances (Å), and results of the IRC calculation for related transition state.

According to mechanism **B**, step 6 for acetylacetonate mono-*S*-methylisothiosemicarbazone is identical to step 6 for methyl acetoacetate *S*-methylisothiosemicarbazone.